Journal of Magnetism and Magnetic Materials 539 (2021) 168364

Contents lists available at ScienceDirect

Journal of Magnetism and Magnetic Materials

journal homepage: www.elsevier.com/locate/jmmm

Research articles

Polymorphism induced magnetic transitions in $Ni(OH)_2$ nanostructures

B. Gokul [a,*], P. Matheswaran [a], M. Pandian [a], C. Arun Paul [b], K. Ravikumar [c], V. Gopala Krishnan [d], Mohd. Shkir [e], S. AlFaify [e], Gedi Sreedevi [f,*]

[a] Department of Physics, Kongunadu Arts and Science College, Coimbatore 641029, Tamil Nadu, India
[b] Department of Science and Humanities, Sri Krishna College of Engineering and Technology, Kuniamuthur, Coimbatore 641008, Tamil Nadu, India
[c] Department of Physics, Vivekanandha College of Arts and Science for Women, Tiruchengode 673205, Tamil Nadu, India
[d] Department of Physics, Dr N.G.P. Arts and Science College, Coimbatore 641048, Tamil Nadu, India
[e] Advanced Functional Materials & Optoelectronics Laboratory (AFMOL), Department of Physics, Faculty of Science, King Khalid University, Abha 61413, Saudi Arabia
[f] School of Chemical Engineering, Yeungnam University, Gyeongsan 38541, Republic of Korea

ARTICLE INFO

Keywords:
Nickel hydroxide
Polymorphism
Complexing agent
Magnetic properties

ABSTRACT

The article describes the impact of complexing agent on the phase changing property of $Ni(OH)_2$ nanostructures (NSs). $Ni(OH)_2$ was prepared by facile hydrothermal method and polymorphism have been obtained by employing two different complexing agent while keeping other parameters constant during synthesis. The α-and β-$Ni(OH)_2$ NSs phase was formed confirmed by XRD and FTIR. FESEM and TEM images reveals that the 3D-flower like α-$Ni(OH)_2$ nanostructure and formation randomly oriented nanopetals of β-$Ni(OH)_2$ NSs. Magnetic features of both α-and β-$Ni(OH)_2$ phases were studied using SQUID magnetometer. α-and β-$Ni(OH)_2$ exhibit blocking temperature at 6 K and 25 K, correspondingly and irreversible hysteresis behavior below blocking temperature. α-$Ni(OH)_2$ shows paramagnetic to superparamagnetic transition whereas β-$Ni(OH)_2$ shows paramagnetic to antiferromagnetic transition as temperature varies from 2 to 50 K.

1. Introduction

Multifunctional properties of layered double hydroxide nanomaterials generate much interest due to its potential applications. The physical and chemical properties of these layered double hydroxide materials were determined by its structure. Among Layered double hydroxides, $Ni(OH)_2$ find potential applications in Ni-based rechargeable batteries, electrochemical supercapacitors, as magnetic material, etc. [1]. $Ni(OH)_2$ is a isostructural compound which can exist in two polymorphism via α- and β phase. Both α- and β phases crystallizes in hexagonal structure with stacked layers and usually forms as thin flakes/platelets [2]. α-$Ni(OH)_2$ (will be referred as ANH) has hexagonal hydrotalcite-like structure with intercalated anions and water molecules, however β-$Ni(OH)_2$(will be referred as BNH) crystallizes in hexagonal structure without intercalated anions and water molecules [3]. Compared to BNH phase, ANH has disordered stacking layers with large C-axis size 7.5–32 Å [4]. To date, different solution methods has been employed to synthesis both ANH and BNH nanostructures (NSs). In the typical synthesis of $Ni(OH)_2$ NSs, no precipitation occurs when simply the Ni ion precursors are used [5]. To induce the nucleation of $Ni(OH)_2$ complexing agent is necessary. Hence complexing agent playing a significant role in construction and phase confirmation of $Ni(OH)_2$ NSs. Control over the phase transformation can be easily obtained by using different complexing agent and also by varying its concentration. This would lead us to prepare highly stable $Ni(OH)_2$ NSs that would not undergo instant phase transformation. Complexing agents like NH_3 [6], urea [7], NaOH [8], ethylenediamine [9], hexamethylenetetramine [10] has been used to synthesis both ANH and BNH nanostructures. Polymorphism also induced by varying the synthesis temperature and by addition of extra co-ordination agents and its influence on the electrochemical properties of $Ni(OH)_2$ were studied [11]. To the best of our knowledge no report is available on the complexing agent induced polymorphism. Extensive amount of work is reported on electrochemical properties of $Ni(OH)_2$ but magnetic features of $Ni(OH)_2$ are rarely reported. The reports are also controversial to each other that Tiwari *et al.* [12] reported that BNH exhibits paramagnetic to ferromagnetic behavior. Rall *et al.* [13] reported that BNH show metamagnetic behavior and ANH possess paramagnetic to ferromagnetic transition. In the report published by Liu *et al.* [14] magnetic property of ANH was determined as transition from paramagnetic to

* Corresponding authors.
E-mail addresses: gokulbangaru@gmail.com (B. Gokul), drsrvi9@gmail.com (G. Sreedevi).

https://doi.org/10.1016/j.jmmm.2021.168364
Received 18 June 2021; Received in revised form 25 July 2021; Accepted 28 July 2021
Available online 31 July 2021

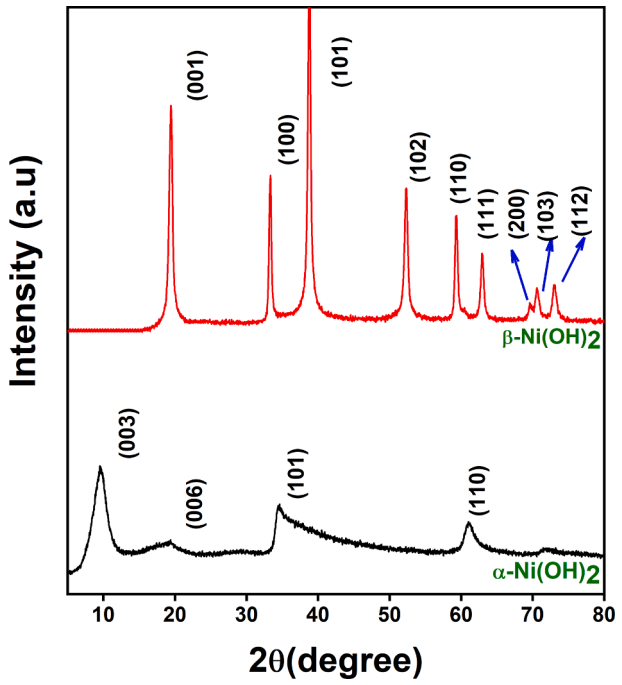

Fig. 1. XRD pattern of ANH and BNH NSs.

antiferromagnetic order. Hence above reports are controversial to each other, which opens opportunities for further investigations.

In this work we have provoked polymorphism in $Ni(OH)_2$ by simply varying complexing agent in reaction with $Ni(NO_3)_2{\cdot}6H_2O$ through facile hydrothermal process and study its magnetic properties.

2. Experimental section

All chemicals Nickel (II) nitrate hexahydrate ($Ni(NO_3)_2{\cdot}6H_2O$-99.99%), Urea (99%) and Ammonia solution 25% (NH_3) used in the synthesis were commercially purchased from Aldrich and used without further purification

2.1. Synthesis of α-and β-Ni (OH) $_2$ NSs

Both ANH and BNH were synthesized through hydrothermal process. First, 0.1 M of $Ni(NO_3)_2{\cdot}6H_2O$ was liquified in 30 ml of deionized (DI) water and stirred (IKA 3,581,000 Ceramic Stirring Hot Plate) in for 15 mins. To the above 0.3 M ratio of urea was added and the mixture was stirred for 30 mins. The solution was poured in to 50 ml teflon lined stainless steel autoclave (Techinstro, India) and reserved at 150℃ for 12 hrs. Pale green α-$Ni(OH)_2$ (ANH) precipitate was obtained after 12 hrs reaction. The precipitates were filtered and consequently washed with DI water and pure ethanol to remove the impurities. The precipitates were dried at 80℃ in hot air oven (Remi, India) for 4 hrs. To prepare β-Ni $(OH)_2$ (BNH) nanostructures, complexing agent NH_3 solution was replaced instead of urea but other parameters such precursor and its concentration, complexing agent concentration, synthesis temperature and other hydrothermal processing parameters were kept same.

2.2. Characterization

Phase structure of the prepared nanostructures was examined by X-ray Diffraction (XRD) using a Shimadzu-6000 XRD working at 40/30 kV/mA own Cu-Kα radiation (1.5406 Å) at 0.02°/s scanning speed over 4–80° angular region. A Shimadzu Prestige-21 Fourier-transform infrared (FTIR)-spectrometer was employed over 400–4000 cm^{-1} range to record vibrational profiles. A Field Emission Scanning Electron

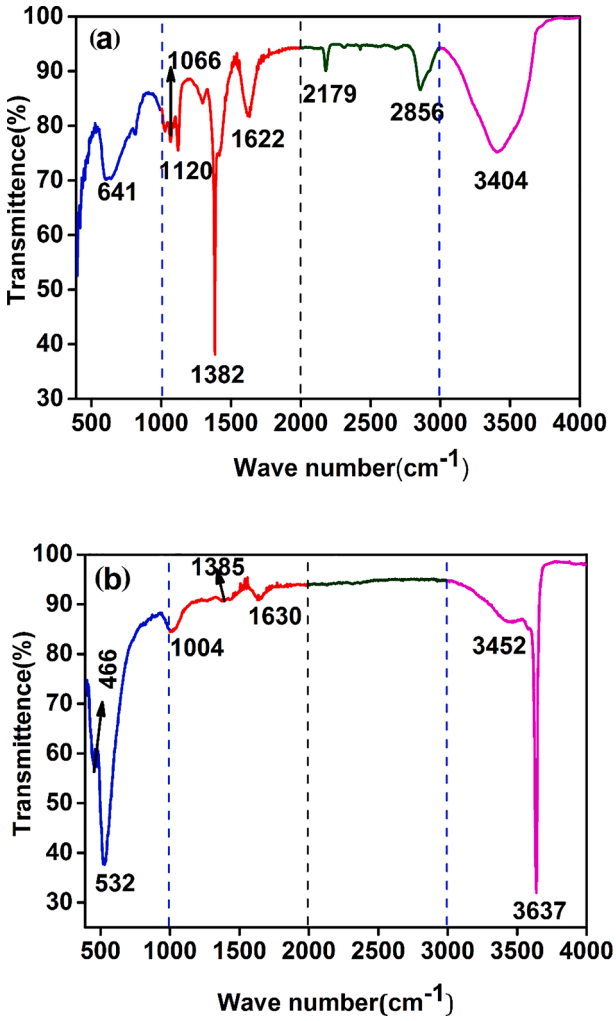

Fig. 2. FTIR spectra of (a) ANH and (b) BNH NSs.

Microscope (FESEM) -SUPRA 55 (Germany) and Philips CM200 Transmission Electron Microscope (TEM), were used for morphological/ Selected Area Electron Diffraction (SAED) analysis. Magnetic properties of the nanoparticles were studied using Ever Cool Superconducting Quantum Interference Device (SQUID) magnetometer as role of both temperature (2–300 K) and applied magnetic field (M-H Curve −5T to 5 T) for different temperatures such as 2 K, 5 K, 10 K, 20 K, 30 K and 50 K.

3. Results and discussion

3.1. Structural property

Polymorphism was identified from structural property analyzed by X-ray diffraction. The phase modification is observed due to the difference in alkaline medium. Difference in alkaline medium was induced by two different complexing agents such as ammonia and urea. Ammonia as complexing agent, induced BNH phase and urea as complexing agent induces ANH phase. Fig. 1 displays the XRD profiles of both ANH and BNH NSs. From the XRD plots the $Ni(OH)_2$, BNH phase has well oriented intense crystalline peaks with hexagonal structure can be indexed to 2θ = 19.25°, 33.06°, 38.53°, 39.09°, 52.09°, 59.05°, 62.72°, 69.34°,70.47°,73.12° corresponds to the planes (001), (100),(101), (002), (102), (110), (111), (200), (103), (112) respectively with lattice parameter a = 3.02 Å, c = 4.65 Å [13]. α- $Ni(OH)_2$ exhibits low intense asymmetry peaks at 2θ = 9.62°, 19.52°, 34.64°, 61.10° indexed to the planes (003), (006) (101) and (110) respectively. This asymmetry peaks due to

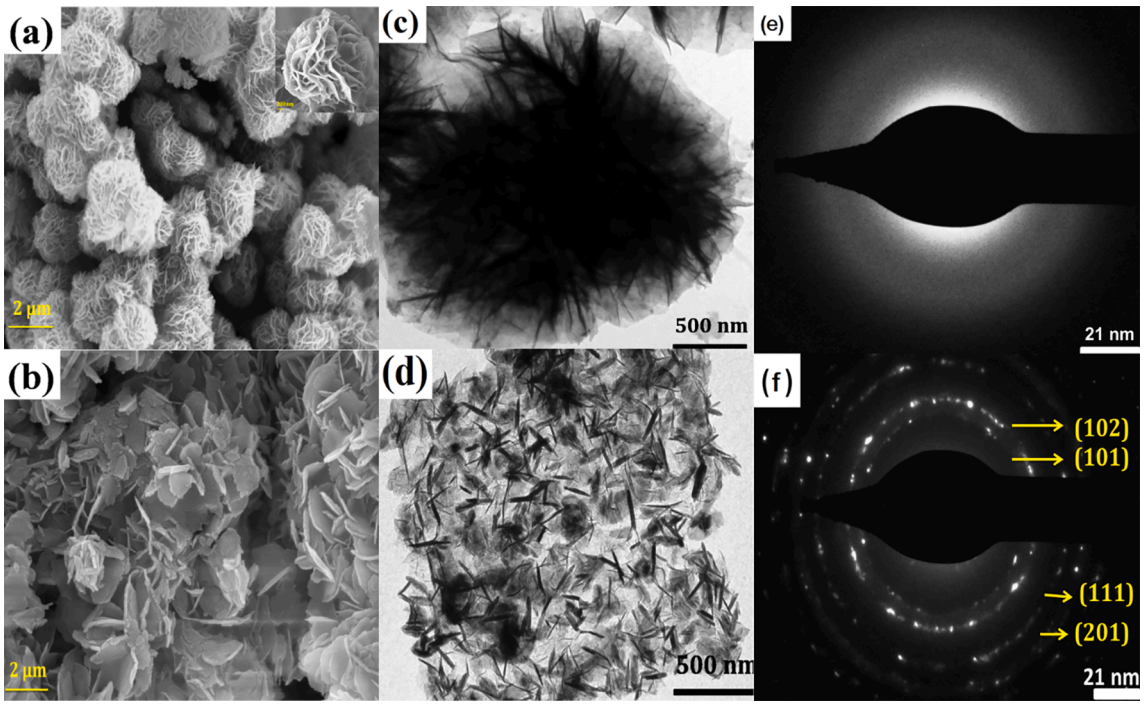

Fig. 3. FESEM images of (a) ANH and (b) BNH NSs, TEM images of (c) ANH and (d) BNH NSs, SAED pattern of (e) ANH and (f) BNH NSs.

intercalated anions(OCN, CO_3^{2-}, OH^-) groups and water molecules between layered structures [15] leading to large lattice parameter a = 3.11 Å, c = 27.7 Å [13]. The broad diffraction peaks suggested the nanocrystalline peaks of $Ni(OH)_2$, the mean crystallite size was estimated from Scherrer formula and noticed to be 6 and 14 nm for ANH and BNH respectively. From the XRD pattern it is apparent that both phases are polycrystalline nature and no other peaks that corresponds to impurity was detected.

3.2. FTIR analysis

FTIR spectra (Fig. 2(a and b)) gives the information about the functional groups present in the prepared ANH and BNH NSs. Fig. 2(a) shows vibrations at 3404 cm^{-1}, 2856 cm^{-1}, 2179 cm^{-1}, 1622 cm^{-1}, 1382 cm^{-1}, 1120 cm^{-1}, 1066 cm^{-1}. The broad band at 3404 cm^{-1} is owed to H-O–H bond stretching of H_2O in ANH NSs. Peak detected at 1622 cm^{-1} belongs to the bending vibrations of the water molecules [15]. A small peak at 2856 cm^{-1} corresponds to symmetric vibrations of - CH_2 – group of urea. Small sharp peak at 2179 cm^{-1} belongs to N-bonded –NCO [16]. The absorption bands at 1066 cm^{-1} are accredited to vibrational mode of C-N. Absorption band located at 1382 cm^{-1} attributed to interlayer nitrate anion. Band at 640 cm^{-1} correspond to Ni-O–H bending vibrations of ANH NSs [17].

Vibrations at 3637 cm^{-1}, 3452 cm^{-1}, 1630 cm^{-1}, 1385 cm^{-1}, 1004 cm^{-1}, 532 cm^{-1}, 466 cm^{-1} observed for BNH nanostructures (Fig. 2(b)). Fine and shrill peak at 3637 cm^{-1} is $\upsilon_{O\text{-}H}$ stretching vibration. The band at 3452 cm^{-1} is hydroxyl groups stretching vibration. 1630 cm^{-1} is the bending vibration of H_2O. Weak absorption band at 1004 cm^{-1} belongs to CO_3^{2-} ions. Band observed at 532 cm^{-1} correspond to hydroxyl groups which particularly appears for BNH NSs [18].

Comparing FTIR Spectra of both ANH and BNH, it is clearly observed that ANH have intercalated ions and also composed different stretching and bending vibrations in the finger print region. Few vibrations peaks are similar may due to same precursor and solvent used to obtain ANH and BNH NSs.

3.3. Surface morphology

Morphological features of prepared hydroxides were recorded using FESEM analysis. FESEM images of ANH reveals (Fig. 3(a)) 3D-flower like structure whose diameter is 3 μm. 3D-flower like structure is assembly of nanopetals of thickness 20–30 nm and wide 2 μm. After 6 hrs of reaction time, these nanopetals connect with each other through centre to form 3D flower like ANH. Urea acts a critical role in developing of 3D flower like architecture. FESEM images of BNH (Fig. 3(b)) show only the presence of nanopetals joined with each other in random manner. There is no formation of 3D flower like architecture even after the 6 hrs reaction time. TEM images (Fig. 3(c and d) produce substantial evidence for the FESEM images, where Fig. 3(c) TEM image of ANH shows the 3D flower like architecture. TEM image of BNH nanostructures Fig. 3(d) shows the two or more nanopetals joined in irregular manner and distributed through interconnection with each other. Due to high alkaline medium, BNH structure rapidly minimizes the surface energy than ANH. No characteristic electron diffraction pattern has been observed from the SAED Pattern (Fig. 3(e)) of ANH. This might be due to the asymmetric band and due to presence of intercalated ions in ANH. SAED pattern of BNH (Fig. 3(f)) nanostructures show characteristic diffraction peaks due to high crystalline nature and are good agreement with X-ray diffraction pattern of BNH.

3.4. Magnetic property

Temperature dependence on magnetization curve of ANH and BNH NSs were measured in the range of 2–400 K in both ZFC and FC(100 Oe) conditions. Both ZFC and FC curve of ANH (Fig. 4(a)) show a steady raise below the bifurcation temperature of 20 K. ANH shows paramagnetic behavior above the bifurcation temperature. Both ZFC and FC curve show maximum at 6 K which is said to be blocking temperature (T_b). Below blocking temperature field cooling magnetization get saturated due to the freezing process of ferromagnetic moments [1]. In case of BNH (Fig. 4(b)), ZFC show a maximum at 25 K, which is near to the bulk value Neel temperature of BNH. Distinct from ANH, only there is rapid increase in FC magnetization curve below blocking temperature (25 K). Observing temperature dependent magnetization curve, it is clear that

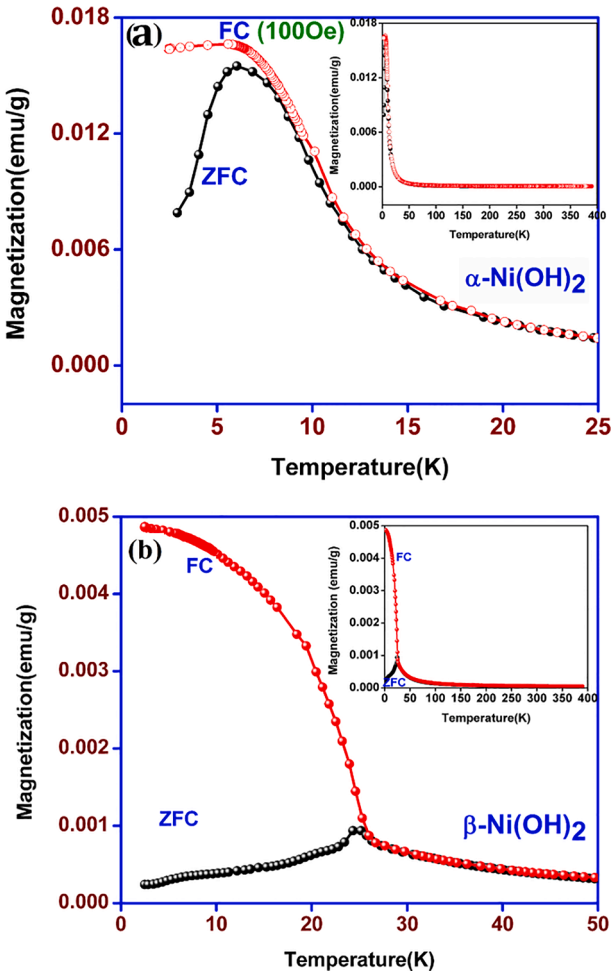

Fig. 4. Temperature dependence curve on magnetization of (a) ANH and (b) BNH NSs under FC (100Oe) and ZFC (Inset- temperature dependence curve on magnetization for full temperature scale 2–400 K).

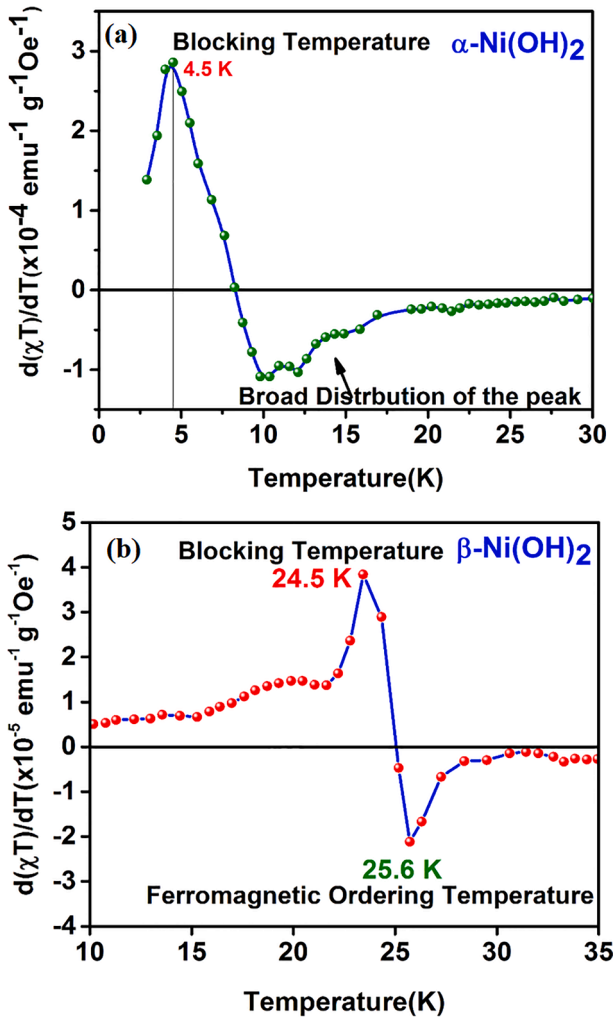

Fig. 5. d(χT)/dT vs T plots of (a) ANH and (b) BNH NSs.

both ANH and BNH have different magnetic behaviors. There is a large difference in the bifurcation temperature (20 K) and blocking temperature (6 K) for ANH, whereas there is no considerable difference is observed for BNH nanostructures. In order to study the magnetic ordering of $Ni(OH)_2$ NSs precisely the derivative of the product of susceptibility and temperature was plotted. The plot of d(χT)/dT vs T are shown in the Fig. 5(a and b) for ANH and BNH NSs respectively. As observed, the positive maximum at the low temperatures represents the blocking temperature of the magnetic nanoparticles and the negative minimum observed at higher temperature is due to FM ordering of the nanoparticles. In the Fig. 5(a), a sharp peak is observed at positive maximum at 4.5 K gives the exact blocking temperature of the ANH but the broad distribution of the negative minimum is anomalous behavior of the nanoparticles. Hence, derivative graph (Fig. 5(a)), clearly demonstrate the absence of the ferromagnetic ordering at lower temperature in ANH. For BNH (Fig. 5(b)) both positive maximum and negative minimum peaks are clearly observed. Positive maximum peak at 24.5 K demonstrates the exact blocking temperature of the BNH phase and negative minimum observed at higher temperature about 25.6 K is FM ordering of Ni^{2+} spins of the BNH. Hence the derivative peaks of ANH show the absence of ferromagnetic ordering and BNH show FM ordering at lower temperature.

Magnetic hysteresis was recorded for different temperatures such as 2 K, 5 K, 10 K, 20 K, 30 K and 50 K. It is apparent that magnetic hysteresis curves of ANH (Fig. 6(a)) and BNH (Fig. 6(b)) show distinct behavior in the measured temperature range. Although both ANH and BNH show irreversible behavior below the blocking temperature, ANH curve shows a ferromagnetic saturation behavior for temperatures 2 K–30 K. Above 30 K, hysteresis shows paramagnetic features. Saturation behavior of nanoparticles without any coercive field is a usual behavior of superparamagnetic nanoparticles. S.D. Tiwari *et al.* [12] reported the transition from *para*-to-ferro-magnetic and superparamagnetic blocking at low temperatures in these $Ni(OH)_2$ NSs. It is been said that superparamagnetic particle may get easily saturated at lower fields. Similar behavior is also observed for ANH (Fig. 6(a)). BNH NSs show linear increase in M value with H showing irreversible features at low temperature. This would be due to antiferromagnetic order of BNH [19]. The irreversible mechanism in antiferromagnetic material can be attributed to the relaxation of disordered magnetic moments on the surface [20]. The coercivity and hysteresis is seen for the temperatures 2, 5, 10 and 20 K and hysteresis completely vanishes at 30 K, hence the ferromagnetic order exists up to 25.6 K as evidenced from the Fig. 6(b) of BNH NSs and coincide with M−T curves. Large coercivity of about 1 KOe is observed for 2 K and lower of about 390 Oe is observed for 20 K. Hence ANH show paramagnetic to superparamagnetic transition and BNH show paramagnetic to antiferromagnetic transition in dependence with temperature. The magnetic transition of the two phases were attributed to their large variation in the c-axis (ANH – 27.7 Å; BNH- c = 4.65 Å) parameter which is function of various intercalated molecules influencing the exchange interaction between Ni^{2+} ions.

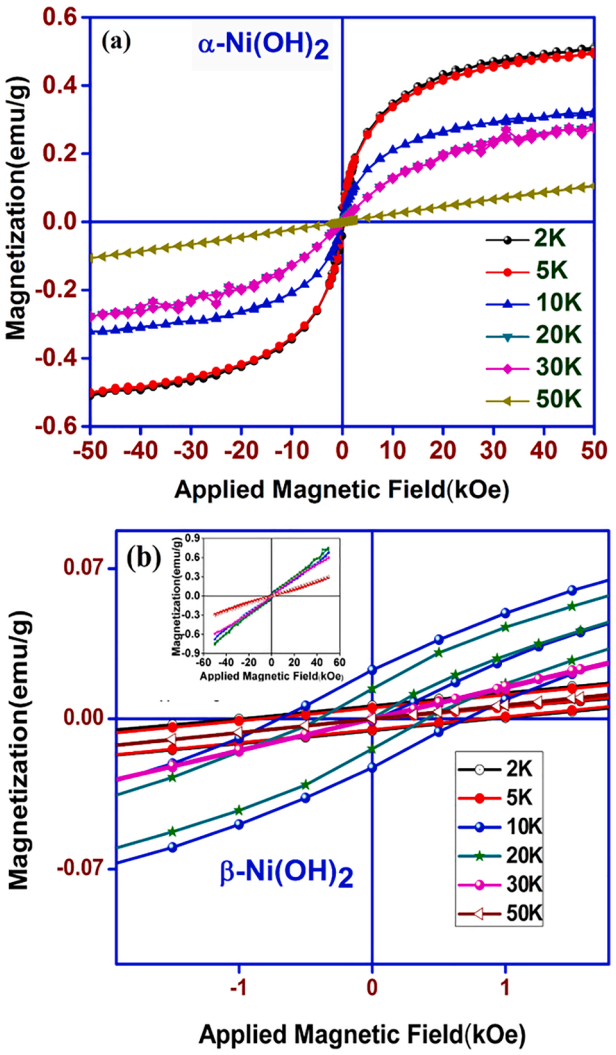

Fig. 6. Hysteresis loops of (a) ANH and (b) BNH NSs for different temperatures (Inset shows hysteresis curve BNH NSs at high field).

4. Conclusion

Significance of complexing agent in the phase transformation of layered hydroxide nanostructures has been studied. Two different phases such as, α-and β-$Ni(OH)_2$ nanostructures are synthesized by simply varying the complexing agent via hydrothermal route. This phase transformation is caused by the difference created in the alkaline medium due to the addition of complexing agent. Magnetic features of α-and β-$Ni(OH)_2$ NSs compounds are different, which can be attributed to their difference in the c-axis of hexagonal crystal structure.

5. Data availability statement

The raw/processed data required to reproduce these findings cannot be shared at this time as the data also forms part of an ongoing study.

Declaration of Competing Interest

The authors declare that they have no known competing financial interests or personal relationships that could have appeared to influence the work reported in this paper.

Acknowledgement

Authors BG, PM acknowledges The Management, Kongunadu Arts and Science College for providing experimental facilities for this work. The authors extend their appreciation to the Deanship of Scientific Research at King Khalid University for funding this work through a through Research Groups Program under Grant No. R.G.P.2/60/42.

References

[1] J.D. Rall, M.S. Seehra, The nature of the magnetism in quasi-2D layered α-$Ni(OH)_2$, J. Phys.: Condens. Matter 24 (7) (2012) 076002, https://doi.org/10.1088/0953-8984/24/7/076002.
[2] M.-G. Ma, J.-F. Zhu, J.-X. Jiang, R.-C. Sun, Hydrothermal–polyol route to synthesis of β-$Ni(OH)_2$ and NiO in mixed solvents of 1,4-butanediol and water, Mater. Lett. 63 (21) (2009) 1791–1793, https://doi.org/10.1016/j.matlet.2009.05.037.
[3] Y. Luo, G. Li, G. Duan, L. Zhang, One-step synthesis of spherical α-$Ni(OH)_2$ nanoarchitectures, Nanotechnology 17 (16) (2006) 4278–4283, https://doi.org/10.1088/0957-4484/17/16/046.
[4] X. Zhao, S. Xu, L. Wang, X. Duan, F. Zhang, Exchange-biased $NiFe_2O_4$/NiO nanocomposites derived from NiFe-layered double hydroxides as a single precursor, Nano Res. 3 (3) (2010) 200–210.
[5] J.D. Rall, M.S. Seehra, E.S. Choi, Metamagnetism and nanosize effects in the magnetic properties of the quasi-two-dimensional system β-$Ni(OH)_2$, Phys. Rev. B 82 (2010), 184403, https://doi.org/10.1103/PhysRevB.82.184403.
[6] Y. Li, B. Tan, Y. Wu, Ammonia-Evaporation-Induced Synthetic Method for Metal (Cu, Zn, Cd, Ni) Hydroxide/Oxide Nanostructures, Chem. Mater. 20 (7) (2008) 2602, https://doi.org/10.1021/cm800156j.
[7] B.P. Bastakoti, H.-S. Huang, L.-C. Chen, K.-C.-W. Wu, Y. Yamauchi, Block copolymer assisted synthesis of porous α-$Ni(OH)_2$ microflowers with high surface areas as electrochemical pseudocapacitor materials, Chem. Commun. 48 (2012) 9150–9152, https://doi.org/10.1039/C2CC32945J.
[8] J. Li, R. Yan, B.o. Xiao, D.T. Liang, D.H. Lee, Preparation of Nano-NiO Particles and Evaluation of Their Catalytic Activity in Pyrolyzing Biomass Components, Energy Fuels 22 (1) (2008) 16–23, https://doi.org/10.1021/ef700283j.
[9] G.-T. Zhou, Q.-Z. Yao, X. Wang, J.C. Yu, Preparation and characterization of nanoplatelets of nickel hydroxide and nickel oxide, Mater. Chem. Phys. 98 (2-3) (2006) 267–272, https://doi.org/10.1016/j.matchemphys.2005.09.030.
[10] B.-H. Liu, S.-H. Yu, S.-F. Chen, C.-Y. Wu, Hexamethylenetetramine Directed Synthesis and Properties of a New Family of α-Nickel Hydroxide Organic−Inorganic Hybrid Materials with High Chemical Stability, J. Phys. Chem. B 110 (9) (2006) 4039–4046, https://doi.org/10.1021/jp055970t.
[11] G.-X. Tong, F.-T. Liu, W.-H. Wu, J.-P. Shen, X. Hu, Y. Liang, Polymorphous α- and β-$Ni(OH)_2$ complex architectures: morphological and phasal evolution mechanisms and enhanced catalytic activity as non-enzymatic glucose sensors, CrystEngComm 14 (2012) 5963–5973, https://doi.org/10.1039/C2CE25622C.
[12] S.D. Tiwari, K.P. Rajeev, Paramagnetic to ferromagnetic transition and superparamagnetic blocking in $Ni(OH)_2$ nanoparticles, Phys. Rev. B 77 (2008), 224430, https://doi.org/10.1103/PhysRevB.77.224430.
[13] J.D. Rall, M.S. Seehra, N. Shah, G.P. Huffman, Comparison of the nature of magnetism in α-$Ni(OH)_2$ and β-$Ni(OH)_2$, J. Appl. Phys. 107 (9) (2010) 09B511, https://doi.org/10.1063/1.3358015.
[14] X.H. Liu, W. Liu, X.K. Lv, F. Yang, X. Wei, Z.D. Zhang, D.J. Sellmyer, Magnetic properties of nickel hydroxide nanoparticles, J. Appl. Phys. 107 (8) (2010) 083919, https://doi.org/10.1063/1.3374468.
[15] Self-powered electrochemical deposition of Cu@Ni(OH)2 nanobelts for high performance pseudocapacitors, (n.d.). http://pubs.rsc.org/en/content/articlehtml/2015/ta/c4ta06710j.
[16] H. Wang, J. Gao, Z. Li, Y. Ge, K. Kan, K. Shi, One-step synthesis of hierarchical α-$Ni(OH)_2$ flowerlike architectures and their gas sensing properties for NO_x at room temperature, CrystEngComm 14 (2012) 6843–6852, https://doi.org/10.1039/C2CE25553G.
[17] Y. Li, X. Xie, J. Liu, M. Cai, J. Rogers, W. Shen, Synthesis of α-$Ni(OH)_2$ with hydrotalcite-like structure: Precursor for the formation of NiO and Ni nanomaterials with fibrous shapes, Chem. Eng. J. 136 (2-3) (2008) 398–408, https://doi.org/10.1016/j.cej.2007.06.001.
[18] J. Xiong, H. Shen, J. Mao, X. Qin, P. Xiao, X. Wang, Q. Wu, Z. Hu, Porous hierarchical nickel nanostructures and their application as a magnetically separable catalyst, J. Mater. Chem. 22 (2012) 11927–11932, https://doi.org/10.1039/C2JM30361B.
[19] D.S. Hall, D.J. Lockwood, C. Bock, B.R. MacDougall, Nickel hydroxides and related materials: a review of their structures, synthesis and properties, Proc. R. Soc. A: Math. Phys. Eng. Sci. 471 (2015) 20140792, https://doi.org/10.1098/rspa.2014.0792.
[20] G.F. Goya, H.R. Rechenberg, J.Z. Jiang, Magnetic irreversibility and relaxation in $CuFe_2O_4$ nanoparticles, J. Magn. Magn. Mater. 218 (2-3) (2000) 221–228, https://doi.org/10.1016/S0304-8853(00)00339-5.